

Cosmic ray electron boosted light dark matter: Implications of LZ 2025 data

Sk Jeesun  ^{1,2,*} and Anirban Majumdar  ^{3,†}

¹*State Key Laboratory of Dark Matter Physics,
Tsung-Dao Lee Institute & School of Physics and Astronomy,
Shanghai Jiao Tong University, Shanghai 200240, China*

²*Key Laboratory for Particle Astrophysics and Cosmology (MOE)
& Shanghai Key Laboratory for Particle Physics and Cosmology,
Shanghai Jiao Tong University, Shanghai 200240, China*

³*Department of Physics, Indian Institute of Science Education and Research - Bhopal,
Bhopal Bypass Road, Bhauri, Bhopal 462066, India*

Abstract

Current multi-ton detectors put stringent constraints on the GeV-scale galactic dark matter, pushing the allowed cross-section almost towards the neutrino fog, yet remain mostly insensitive to the light dark matter. Cosmic rays can upscatter the non-relativistic halo dark matter particles, making a sub-population of them gain sufficient kinetic energy to be discernible in current direct search experiments. In this work we explore this alternate strategy to probe sub-MeV electrophilic dark matter boosted by cosmic rays with the latest data of LZ 2025 (WS2024 run) and improve the constraint on the MeV scale dark matter by almost $\sim \mathcal{O}(1)$ compared to previous XENONnT limit for energy-independent cross-section. Using realistic energy-dependent cross-sections, we also analyse such a scenario, where the associated mediator mass plays a crucial role in governing the event rate and hence the expected limits too. With energy-dependent cross-sections, our obtained limits also remain stronger than the existing constraints from current direct detection experiments. Even compared to the limits from the neutrino detectors with a larger target size, LZ 2025 can put stringent constraints in certain parameters space of the mediator, excluding the previously unexplored regions.

Introduction. The quest for the particle nature of the non luminous and non-baryonic dark matter (DM) persists even after the numerous investigations over the past several decades [1, 2]. DM constitutes 25% of the total energy budget of the universe at present and has been strongly indicated by observations relying on its gravitational interactions [3–6]. Despite the strong observational evidence, the non-gravitational interactions of particle DM still remain elusive. Ground-based direct detection (DD) experiments bring an excellent opportunity to trace such galactic DM particles through their scatterings with nucleons or electrons while the Earth traverses through the DM halo [2, 7–10]. Null results in experiments like XENONnT [11], LUX-ZAPELIN (LZ) [12, 13], PandaX-4T [14], DarkSide-50 [15] have placed stringent constraints on the electroweak scale DM and thus motivate the community to seek DM particles in the sub-GeV mass range.

The non-relativistic galactic halo DM particles with MeV scale mass and velocity $\sim 10^{-3}c$ fails to generate a recoil energy above the threshold energy (\gtrsim keV) of the multi-ton detectors making the existing direct searches ineffective in detecting light halo DM particles. To circumvent this deadlock, a subdominant boosted component of light DM with almost relativistic speeds are being explored [16, 17]. MeV-scale DM particles in the halo with electronic or nuclear interactions are expected to inevitably scatter with highly energetic (with energy \gtrsim GeV-TeV) cosmic rays in the galaxy and thus may gain

kinetic energies higher than the experimental thresholds. This sub-population of light DM reaching the Earth-based multi-ton detectors and producing a unique recoil signature may help to resolve the intriguing puzzle of the light DM. Null observations of any such recoil leads to stringent constraint on the respective DM interactions [16–22]. Numerous works in the recent past have explored the novel idea of DM boosted by other mechanisms as well, to probe such light DM interactions. Examples include DM boosted by blazar jet [23–25], diffuse supernova neutrinos [26, 27], supernova emission [28], solar reflection [29, 30].

In this work, we explore an electrophilic light DM boosted by the cosmic ray electrons (CRe) and their possible signature in LZ experiment [13]. LZ, with its recent data from WS2024, which has a 3.2 ton-year exposure, has the potential to probe such low-mass DM parameter space, which serves as the main goal of this work. Existing literature has already shown that the DM recoil signature as well as the obtained limits, change drastically in the presence of a realistic energy-dependent cross-section compared to a constant cross-section [19, 31, 32]. Apart from a constant cross-section, we consider two realistic cross-sections between DM and e: (1) vector mediator and (2) scalar mediator. We emphasize that in such Boosted DM (BDM) scenarios, the mass of the associated mediator particle plays a non-trivial role in governing the recoil rate and, consequently, in the obtained constraints. To give a rigorous example, we present a benchmark vector mediator model and show the constraints in the mediator parameter space. Though multi-ton neutrino detectors like Super Kamiokande and IceCube provide the strongest constraint on such BDM, we show that in cer-

*Electronic address: skjeesun48@gmail.com

†Electronic address: anirban19@iiserb.ac.in

tain parameter space, LZ 2025 [13], with its low threshold energy and sizable exposure, places the world-leading direct detection constraint on MeV-scale electrophilic DM.

Cosmic ray boosted DM flux. A subdominant yet energetic component of the cosmic ray is the cosmic electrons (CRe) as inferred from observation [33]. DM having an interaction channel with electrons is expected to be up-scattered by this CRe, leading to a boosted flux of χ given as [16],

$$\frac{d\Phi_\chi}{dT_\chi} = D_{\text{eff}} \frac{\rho_\chi^{\text{local}}}{m_\chi} \int_{T_e^{\min}(T_\chi)}^{\infty} \frac{d\Phi_e^{\text{CR}}}{dT_e} \frac{d\sigma_{\chi e}}{dT_\chi} dT_e, \quad (1)$$

where $\rho_\chi^{\text{local}} = 0.3 \text{ GeV/cm}^3$ is the local DM density whereas, m_χ and $\sigma_{\chi e}$ signify the DM mass and elastic DM- e scattering cross-section respectively. T_χ and T_e represent the kinetic energy of the boosted (up-scattered) DM and CRe, respectively.

D_{eff} is the effective diffusion zone parameter given by the line of sight (l.o.s.) integral of the galactic DM density profile [16, 19],

$$D_{\text{eff}} = \frac{1}{\rho_\chi^{\text{local}}} \int \frac{d\Omega}{4\pi} \int_0^{\ell_{\max}} \rho_{\text{MW}} d\ell. \quad (2)$$

ρ_{MW} is the DM density distribution in the Milky Way and we consider the conventional Navarro–Frenk–White (NFW) DM profile which is a function of the galactocentric distance along the l.o.s. r [34]. r is given as

$r(\ell, \psi) = \sqrt{r_\odot^2 - 2\ell r_\odot \cos \psi + \ell^2}$, where $r_\odot = 8.5 \text{ kpc}$ and ψ represent the Sun's distance from the Galactic centre and the observation angle, respectively. D_{eff} in principle incorporates the effective distance from Earth, upto which the effects from the CRe-DM scattering are considered. With a NFW profile and integrating over the l.o.s integral upto 1 kpc leads to $D_{\text{eff}} \sim 1 \text{ kpc}$. The

same with an optimistic upper limit up to 10 kpc leads to $D_{\text{eff}} \sim 10 \text{ kpc}$. For this work, we simply consider a homogeneous distribution of the CRe flux as inferred from the local observations, with $D_{\text{eff}} = 1 \text{ kpc}$ for the conservative limit [16, 19].

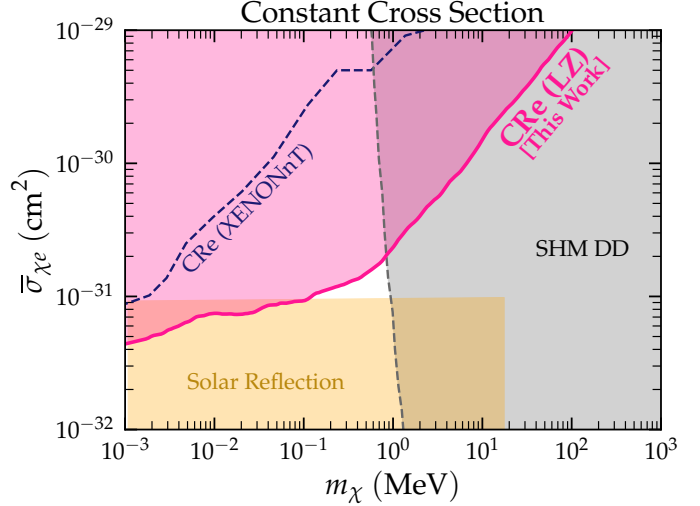


FIG. 1: 2σ C.L. constraints on CRe boosted DM with **constant** cross-section from LZ 2025 is shown by purple shaded region. Existing constraints from BDM search at XENONnT [35] (dashed blue line), solar reflected DM [29] (orange shaded region) and the combined DD limits from SuperCDMS [36], SENSEI [37], and XENON10 [38] for galactic halo DM (grey shaded region) are also shown.

The term $d\Phi_e^{\text{CR}}/dT_e$ in eq.(1) signifies the local interstellar flux of cosmic electrons and is obtained from the observations in experiments like Voyager [39], Fermi-Lat [40], PAMELA [5], AMS-02 [41]. Fitting the observational data the CRe flux is obtained as [20, 33, 42],

$$\frac{d\Phi_e^{\text{CR}}}{dT_e d\Omega} = \begin{cases} \frac{1.799 \times 10^{44} T_e^{-12.061}}{(1 + 2.762 \times 10^{36} T_e^{-9.269} + 3.853 \times 10^{40} T_e^{-10.697})} & \text{for } T_e < 6880 \text{ MeV} \\ \frac{3.259 \times 10^{10} T_e^{-3.505}}{3.204 \times 10^5 T_e^{-2.620}} & \text{for } T_e \geq 6880 \text{ MeV} \end{cases} \quad (3)$$

in units of $\text{sr}^{-1} \text{m}^{-2} \text{s}^{-1} \text{MeV}^{-1}$, where T_e is given in MeV. As mentioned earlier, we treat this flux to be homogeneous with $D_{\text{eff}} = 1 \text{ kpc}$.

The minimum kinetic energy of CRe required to boost a non-relativistic DM to energy T_χ is denoted as T_e^{\min} in eq.(1) and is given as [16],

$$T_e^{\min}(T_\chi) = \left(\frac{T_\chi}{2} - m_i \right) \left[1 \pm \sqrt{1 + \frac{2T_\chi(m_i + M_\chi)^2}{M_\chi(2m_e - T_\chi)^2}} \right], \quad (4)$$

The +ve (−ve) sign in the above equation applies when $T_\chi > 2m_i$ ($T_\chi < 2m_i$).

The BDM flux in eq.(1) has a crucial dependence also on the differential cross-section between e and χ where the underlying Lorentz structures of the BSM interaction between DM and e come into play. In accordance with the GeV scale non-relativistic (NR) DM scattering, usually the energy-independent differential cross-section between CRe and χ is considered in the literature which reads as [16],

$$\frac{d\sigma_{\chi e}}{dT_\chi} = \frac{\bar{\sigma}_{\chi e}}{T_\chi^{\max}}. \quad (5)$$

T_χ^{\max} is the maximum kinetic energy χ can achieve after the scattering, given as

$$T_\chi^{\max} = \frac{T_e^2 + 2m_e T_e}{T_e + (m_e + m_\chi)^2/(2m_\chi)}. \quad (6)$$

Since CRe has sufficient energy to boost a light (sub-

GeV) DM to gain almost semi-relativistic velocities, the differential cross-sections may differ significantly in cases where kinetic energy of the incoming (or, the target) particle appears in the amplitude often referred as energy-dependent cross-sections [18, 20]. This often leads to significant alteration in the obtained limits, especially in the low DM mass region, compelling us to consider the energy-dependent cross-sections as well. In this work, we consider the scalar and vector mediated DM-e scattering whose differential cross-sections read as,

$$\begin{aligned} \left(\frac{d\sigma_{\chi e}}{dT_\chi} \right)_{\text{scalar}} &= \bar{\sigma}_{\chi e} \left(\frac{m_\chi}{4\mu_{e\chi}^2} \right) \frac{(2m_\chi + T_\chi)(2m_e^2 + m_\chi T_\chi)}{s_{\text{CR}} T_\chi^{\max}} F_{\text{DM}}^2(q^2) \\ \left(\frac{d\sigma_{\chi e}}{dT_\chi} \right)_{\text{vector}} &= \bar{\sigma}_{\chi e} \left(\frac{m_\chi}{2\mu_{e\chi}^2} \right) \frac{(2m_\chi(m_e + T_e)^2 - T_\chi((m_e + m_\chi)^2 + 2m_\chi T_e) + m_\chi T_\chi^2)}{s_{\text{CR}} T_\chi^{\max}} F_{\text{DM}}^2(q^2), \end{aligned} \quad (7)$$

respectively, with $\mu_{e\chi}$ being the reduced mass of $\chi - e$ system. $s_{\text{CR}} = (m_\chi + m_e)^2 + 2m_\chi T_e$ is the center of momentum energy of $\chi - e$ scattering. $F_{\text{DM}}(q^2)$ incorporates the information of the mass scale of the mediator participating in the aforementioned interaction, given as,

$$F_{\text{DM}}(q^2) = \frac{q_{\text{ref}}^2 + m_{\text{med}}^2}{q^2 + m_{\text{med}}^2}, \quad (8)$$

with $q = \sqrt{2m_\chi T_\chi}$ being the associated 3-momentum transfer. $q_{\text{ref}} = \alpha m_e$ is the reference momentum to define the NR cross-section $\bar{\sigma}_{\chi e}$. m_{med} is the mediator mass. Note that for $m_{\text{med}} \gg q$ ($m_{\text{med}} \ll q_{\text{ref}}$) i.e. in heavy (light) mediator limit $F_{\text{DM}}(q^2)$ reduces to 1 ($(\alpha m_e/q)^2$).

Recoil spectra. Upon arriving the Earth-based underground DM detector such BDM particles will scatter with the target electrons and produce recoil signature. The expected event rate is calculated as,

$$\frac{dR_{\chi e}}{dE_R} = t_{\text{exp}} n_{\text{T}} \mathcal{E}(E_R) Z_{\text{eff}}(E_R) \int_{T_\chi^{\min}(E_R)}^{T_\chi^{\max}} dT_\chi \frac{d\Phi_\chi}{dT_\chi} \frac{d\sigma_{\chi e}}{dE_R}, \quad (9)$$

where the recoil energy of target electron, the experimental run time and the number of target atomss are represented as E_R , t_{exp} and n_{T} respectively, while the binding energy effects of atomic electrons in xenon are incorporated through the effective charge function $Z_{\text{eff}}(E_R)$. Following Ref. [43], this function is approximated using a series of step functions that account for the ionization thresholds of individual atomic shells, and is expressed as $Z_{\text{eff}}(E_R) \approx \sum_{i=1}^{54} \Theta(E_R - \mathcal{B}_i)$, where $\Theta(x)$ denotes the Heaviside step function. The quantities \mathcal{B}_i correspond to the single-particle binding energies of the i th electron in the xenon atom, evaluated using Hartree-Fock atomic structure calculations as reported in Ref. [43].

$\mathcal{E}(E_R)$ encodes the detector efficiency as a function of recoil energy. In this work, $\mathcal{E}(E_R)$ is taken from the publicly reported 1D region-of-interest (ROI) efficiency curve shown in Fig. 1 of the LZ WS2024 data release [13], which incorporates the combined effects of trigger response, S1 threshold requirements, single-scatter reconstruction, and data analysis selection cuts. T_χ^{\min} stands for the minimum kinetic energy of χ need to scatter an electron with a recoil energy E_R and can be found from eq.(4) with the substitution $T_\chi \rightarrow T_e$, $m_e \rightarrow m_\chi$ and $m_\chi \rightarrow m_e$ [16].

Here also, the differential scattering cross-section between the incoming energetic DM and the target electron at rest, plays the crucial role in the event rates. For energy independent amplitude the differential cross-section is given as [16],

$$\frac{d\sigma_{\chi e}}{dE_R} = \frac{\bar{\sigma}_{\chi e}}{E_R^{\max}}. \quad (10)$$

E_R^{\max} is the maximum kinetic energy gained by the target electron and is given by

$$E_R^{\max} = \frac{T_\chi^2 + 2m_\chi T_\chi}{T_\chi + (m_e + m_\chi)^2/(2m_e)}. \quad (11)$$

The same cross-sections with target electrons for scalar and vector mediator can be obtained from earlier discussed eq.(7) with the substitution $T_\chi \rightarrow T_e$, $m_e \rightarrow m_\chi$, $m_\chi \rightarrow m_e$, $T_\chi^{\max} \rightarrow E_R^{\max}$ and $s_{\text{CR}} \rightarrow s_\chi = (m_\chi + m_e)^2 + 2m_e T_\chi$ (see eq.(A1)-eq.(A2)).

To simulate the events, we use the updated WS2024 data from the LZ collaboration corresponding to their 1D ROI likelihood analysis in reconstructed energy, published in 2025 with a total exposure of 3.3 ton \times year [13].

To obtain the reconstructed event spectra we use the smearing,

$$\frac{dR_{\chi e}}{dT_{\text{er}}^{\text{reco}}} = \int_0^{E_R^{\text{max}}} dE_R \frac{dR_{\chi e}}{dE_R} \mathcal{G}(E_R, T_{\text{er}}^{\text{reco}}), \quad (12)$$

$T_{\text{er}}^{\text{reco}}$ and $\mathcal{G}(E_R, T_{\text{er}}^{\text{reco}})$ are the reconstructed electron recoil energy and the Gaussian smearing function respectively. We consider the resolution power $\sigma = 0.323\sqrt{E_R^{\text{reco}}}$ keV [44]. Plugging the BDM flux from eq.(1) in eq.(9) and then after smearing in eq.(12) we obtain the events in each bin for a fixed set of m_χ and $\bar{\sigma}_{\chi e}$. To place the constraints, we follow the state-of-the-art calculation to find the χ^2 value at each point on the m_χ vs. $\bar{\sigma}_{\chi e}$ plane and then marginalize it to get $\Delta\chi^2 = \chi^2 - \chi^2_{\text{min}} = 6.18$ for 2σ confidence level (C.L.) limit. χ^2_{min} is the minimum value of the whole set. A detail discussion about the recoil spectra and χ^2 analysis can be found in Appendix A and Appendix B.

Constraints. We show our limits obtained at 2σ C.L. from LZ 2025 in Fig.1, considering a constant cross-section depicted by the purple shaded region. We also showcase the existing limit on CRe boosted DM from XENONnT [35] shown by dashed blue lines. Our obtained limit excludes $\sim \mathcal{O}(1)$ smaller $\bar{\sigma}_{\chi e}$ than the XENONnT for $m_\chi \sim 0.1$ MeV. With a decrease in m_χ the bound on $\bar{\sigma}_{\chi e}$ becomes stronger because of the higher amount of incoming BDM flux for light χ [20]. Complementary bound from solar reflected DM [30] (orange shaded region) and the combined DD limits from SuperCDMS [36], SENSEI [37], and XENON10 [38] for galactic halo DM (grey shaded region) are also portrayed for comparison.

The constraints on CRe boosted DM change drastically while considering energy dependent cross-sections. To investigate these phenomena we consider the earlier mentioned two scenarios: vector and scalar mediated interaction between DM and e . While analysing the energy dependent cross-sections the mass scale of the associated mediator is crucial in deciding the BDM flux and the recoil spectra. We first display our 2σ C.L. constraints in the heavy mediator limit i.e. $F_{\text{DM}}(q) = 1$ obtained from LZ 2025 in Fig.2 for (a) vector mediator (**left panel**) and (b) scalar mediator (**right panel**). To signify our limits and existing constraints we follow the same color convention as discussed earlier. The combined DD limits [36–38] for galactic halo DM (grey shaded region) are also shown for both of the aforementioned plots. For vector mediator scenario, our obtained limit is stronger than the earlier bound from XENONnT [35] (dashed blue line) by almost factor ~ 2 . Since we do not find any XENONnT analysis in the existing literature with scalar mediator we portray the older XENON1T limit for comparison. It is worth highlighting that, in the heavy mediator limit LZ 2025 constraints with energy dependent cross-sections are order of magnitude stronger than the same with constant cross-section. On the other hand, the LZ limit obtained with a scalar mediator (**right panel**) is weaker

than that with vector mediator (**left panel**) in low mass ($m_\chi \lesssim 10^{-1}$ MeV) range. This can be perceived from the associated E_R suppression (see eq.(A1)) in the differential cross-section for scalar mediator [20].

The incoming BDM flux with high cross-section with matter is expected to be affected by Earth's attenuation while traversing through it before reaching the underground detector. Using analytical estimations, it can be understood that attenuation places an upper roof on the cross-section which is around $\sigma_{\chi e} \gtrsim \text{few} \times 10^{-28}$ cm 2 in the heavy mediator limit [16, 20, 35]. Incoming χ with $\bar{\sigma}_{\chi e}$ larger than the quoted value gets attenuated and fails to generate recoil events in the detector. For simplicity, in this work we do not include the effect of attenuation and show our constraints only upto $\sigma_{\chi e} = 10^{-29}$ cm 2 for the heavy mediator limit.

On the other hand, 2σ C.L. constraints from LZ 2025 in the light mediator limit i.e. $F_{\text{DM}}(q) = (\alpha m_e)^2/q^2$ are shown in Fig.3 for (a) vector mediator (**left panel**) and (b) scalar mediator (**right panel**). Again, we follow the same color convention to represent the obtained limits and the existing constraints. Note that, for this scenario, the obtained limits are significantly weaker than those obtained in the heavy mediator limit, due to the suppression in the differential cross-section from F_{DM} . This leads to a significantly smaller amount of incoming BDM flux for $m_\chi \gtrsim 1$ MeV [20] and consequently a suppressed event rate. Note that our obtained limits in this case are also stronger than the previously obtained BDM constraints.

Super kamiokande (Super-k) [20] and IceCube [46] so far set the most stringent constraints on CRe boosted sub MeV DM in the heavy mediator limit, thanks to their humongous target size. For example, for constant cross-section $\bar{\sigma}_{\chi e} \gtrsim 10^{-32}$ cm 2 is excluded from Super-k for $m_\chi \sim 1$ MeV. For vector (scalar) mediated cross-section Super-k excludes $\bar{\sigma}_{\chi e} \gtrsim 10^{-34}$ cm 2 ($\bar{\sigma}_{\chi e} \gtrsim 10^{-33}$ cm 2) for $m_\chi \sim 1$ MeV in the heavy mediator limit [20]. However, in the light mediator limit neutrino detector constraints are significantly weaken. For vector (scalar) mediated cross-section Super-k excludes $\bar{\sigma}_{\chi e} \gtrsim 10^{-29}$ cm 2 ($\bar{\sigma}_{\chi e} \gtrsim 10^{-28}$ cm 2) for $m_\chi \sim 1$ keV in the light mediator limit [20]. The threshold of Super K (IceCube) is $\mathcal{O}(100)$ MeV ($\mathcal{O}(500)$ GeV) which leads to a suppressed ($\sim 1/q^2$) recoil rate in the light mediator limit. On the other hand, LZ benefits from its very low threshold energy (~ 1 keV) and can place stronger constraint in the light mediator limit. Thus in that parameter space, LZ 2025 places the world leading constraint on CRe boosted DM.

Due to the huge differences in different detector thresholds, it is also crucial to properly identify the mediator mass range while comparing the limits from DM and neutrino detectors. For example, “heavy mediator” limit in Super-k signifies the mediator mass to be $\gtrsim \mathcal{O}(100)$ MeV, whereas the same limit in the LZ can be realized when the mediator mass is $\gtrsim \mathcal{O}(100)$ keV. Thus, for concrete analysis, it is essential to consider minimal benchmark DM models featuring the earlier mentioned mediators.

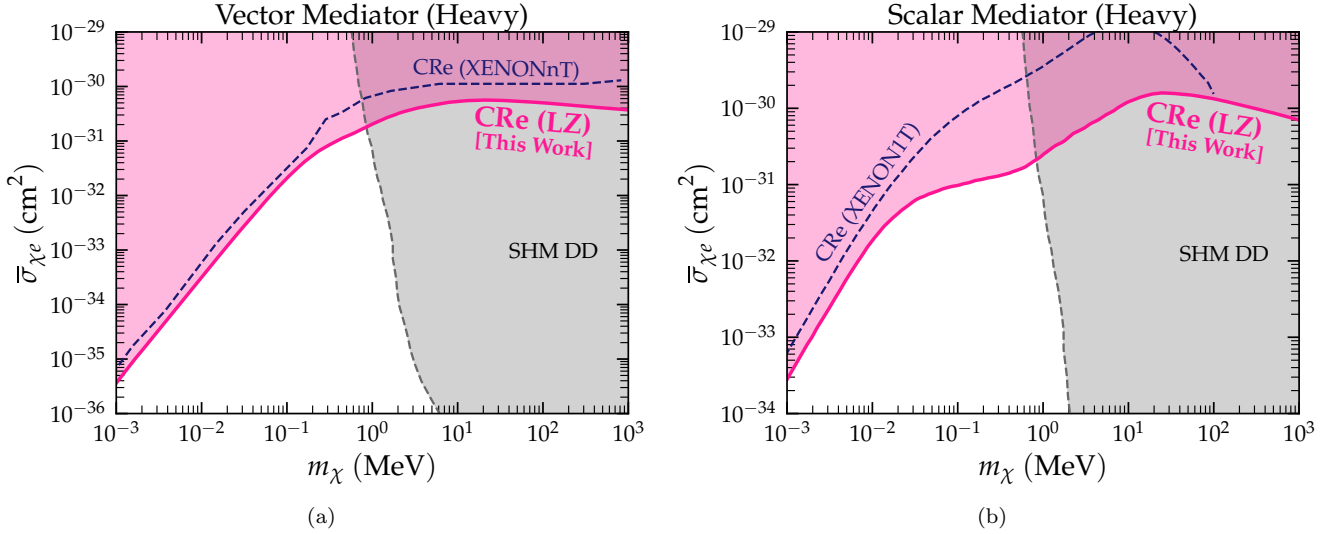


FIG. 2: 2σ C.L. constraints on CRe boosted DM in the heavy mediator limit ($F_{\text{DM}}(q) = 1$) with (a) **vector** mediator and (b) **scalar** mediator from LZ 2025 are shown by purple shaded region. Existing constraints from BDM search at XENONnT [35] (dashed blue line) and the combined DD limits from SuperCDMS [36], SENSEI [37], and XENON10 [38] for galactic halo DM (grey shaded region) are also portrayed.

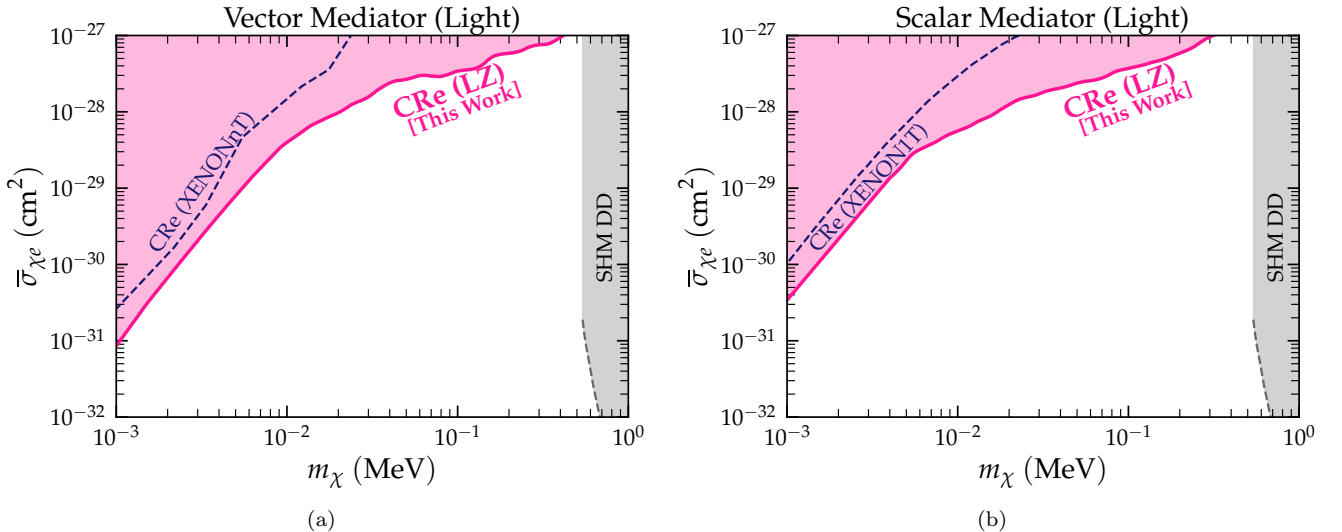


FIG. 3: 2σ C.L. constraints on CRe boosted DM in the light mediator limit ($F_{\text{DM}}(q) = (\alpha m_e)^2/q^2$) with (a) **vector** mediator and (b) **scalar** mediator from LZ 2025 are shown by purple shaded region. Existing constraints from BDM search at XENONnT [35] (dashed blue line) and DAMIC 2025 [45] limit for galactic halo DM (grey shaded region) are also portrayed.

As an example, we choose a minimal model with fermion DM χ and a beyond the standard model (BSM) vector mediator V and write the following lagrangian,

$$\mathcal{L}_{\text{int}} \supset -g_V^\chi \bar{\chi} \gamma^\mu \chi V_\mu - g_V^e \bar{e} \gamma^\mu e V_\mu, \quad (13)$$

g_V^e (g_V^χ) is the respective coupling of V with electron (DM). The mediator mass is denoted as m_V . The reference NR cross-section is then given by,

$$\bar{\sigma}_{\chi e} = \frac{4(g_V^e g_V^\chi)^2 \mu_{\chi e}^2}{\pi (q_{\text{ref}}^2 + m_V^2)^2} \quad (14)$$

In Fig. 4 we present our 2σ C.L. constraints in the vector mediator parameter space (m_V vs. g_V^e plane) for CRe boosted DM from LZ 2025. Here we fix the DM coupling g_V^χ to be 1. We display our exclusion limits for $m_\chi = 1$ MeV, 10 MeV and 100 MeV depicted by the

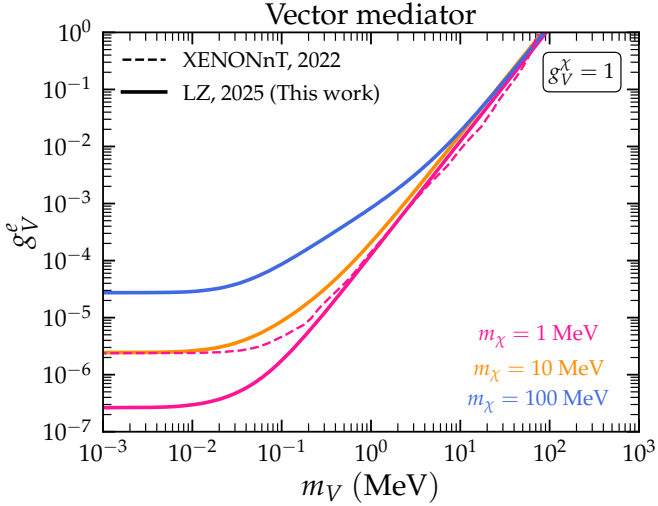


FIG. 4: 2σ C.L. constraints in the **vector** mediator mass vs. coupling parameter space for CRe boosted DM from LZ 2025. Limits corresponding to $m_\chi = 1$ MeV, 10 MeV and 100 MeV are represented by the region above the purple, orange and blue solid lines respectively.

regions above the purple, orange and blue solid lines respectively. For a quick comparison, our obtained limit on $g_{V_e}^e$ for $m_\chi = 1$ MeV at $m_V \lesssim 10^{-2}$ MeV is stronger than XENONnT [35] by a factor ~ 6 . Super-k limit [20] on $g_{V_e}^e$ for $m_\chi = 1$ MeV with $m_V \lesssim 10^{-1}$ MeV is expected to be at least $\mathcal{O}(2)$ weaker than our limit. A similar analysis with scalar mediator can also be performed (see Appendix C).

Complementary bound from solar reflected DM is also applicable for our scenario and is expected to exclude $\sigma_{\chi e} \lesssim 10^{-31} \text{ cm}^2$ and $1 \text{ keV} \lesssim m_\chi \lesssim 10 \text{ MeV}$ [29, 30]. However, in the absence of any rigorous analysis of purely electrophilic solar reflected DM with vector or, scalar mediator in the existing literature, we refrain from showcasing the solar reflected DM limit. For the ultralight mediator case, light mediators are constrained from cooling of astrophysical bodies like Sun, Red Giant (RG) and Supernova [47, 48]. The re-casted limit on the m_χ vs. $\sigma_{\chi e}$ plane, from RG excludes $m_\chi \lesssim 6 \text{ keV}$ for vector mediator and the whole region of interest for the scalar mediator [49]. On the other hand, supernova cooling constrains $10^{-32} \text{ cm}^2 \lesssim \sigma_{\chi e} \lesssim 10^{-38} \text{ cm}^2$ for $m_\chi = 1 \text{ keV}$ for ultralight vector mediator [20, 49]. Despite all these astrophysical bounds, our obtained limit from LZ 2025 is stronger for the light vector mediated DM, whereas the same serves as a complementary direct probe for the light scalar mediated DM. Cosmological constraints from big bag nucleosynthesis (BBN) [50] exclude fermion DM with $m_\chi \lesssim 8 \text{ MeV}$, although they depend on the thermal history and can be surpassed in an extended DM sector. For the light mediators discussed in the context of Fig.4, there also exist constraints from BaBar

($g_{V_e} \gtrsim 10^{-4}$) [51, 52], invisible decay from NA64 [53] and beam dump experiments [52]. The limits from the ground-based detectors depend strongly on the ultraviolet (UV) completion of the benchmark model and change drastically depending on the DM mass and its other interactions. Hence, we refrain from recasting these limits in our parameter space. Our obtained limits are complementary to them and, in some parameter space (for $m_\chi \lesssim 10 \text{ MeV}$, and $m_V \lesssim 1 \text{ MeV}$), stronger than the existing limits. Thus, LZ 2025 data can be extremely helpful for understanding the particle nature of an electrophilic light DM accelerated by the cosmic rays and help to address one of the key puzzles of the universe.

Conclusion. CRe upscattering of light DM makes them detectable in the underground detectors which can probe the previously inaccessible DM parameter space. In this work we provide the updated constraint on such electrophilic DM analysing the latest LZ data [13]. We show that LZ places constraint on DM-e cross-section stronger than previous strongest DD limit from XENONnT [35]. For such boosted DM the energy dependencies in their respective cross-section have a pivotal role in the obtained rates and consequently in the constraints from DD experiments. To scrutinize this issue we also consider realistic cross-sections with minimal DM models featuring vector and scalar mediators. Through exhaustive numerical scans within such frameworks we present the limits obtained from LZ 2025 on CRe boosted DM. We observe that, with the realistic cross-sections, the obtained limits strongly depend on the mediator mass compelling us to rigorously analyze it with realistic models featuring BSM mediators. In the light mediator regime, LZ places the most stringent limit, superseding the bounds from other experiments. In the future, experiments such as DARWIN, JUNO, DUNE and Hyper-kamiokande will frame the pathway of further investigation of the low mass boosted DM parameter space.

Acknowledgement

SJ is supported by the National Natural Science Foundation of China (12425506, 12375101, 12090060, and 12090064) and the SJTU Double First Class start-up fund (WF220442604). AM acknowledges financial support from the Government of India through the Prime Minister Research Fellowship (PMRF) scheme, (ID: 0401970).

Appendix A: Differential cross-section and recoil spectra

The differential cross-section for DM scattering with target electron in the detector is given as,

$$\left(\frac{d\sigma_{\chi e}}{dE_R}\right)_s = \bar{\sigma}_{\chi e} \left(\frac{m_e}{4\mu_{e\chi}^2}\right) \frac{(2m_e + E_R)(2M_\chi^2 + m_e E_R)}{s_\chi E_R^{\max}}, \quad (A1)$$

$$\left(\frac{d\sigma_{\chi e}}{dE_R}\right)_v = \bar{\sigma}_{\chi e} \left(\frac{m_e}{2\mu_{e\chi}^2}\right) \frac{2m_e(M_\chi + T_\chi)^2 - E_R((m_e + M_\chi)^2 + 2m_e T_\chi) + m_e E_R^2}{s_\chi E_R^{\max}}, \quad (A2)$$

for scalar-mediated and vector-mediated cross-section, respectively. For this analysis, we use the following smearing function

$$\mathcal{G}(E_R, E_R^{\text{reco}}) = \frac{1}{\sqrt{2\pi}\sigma} \exp\left(-\frac{(E_R - E_R^{\text{reco}})^2}{2\sigma^2}\right), \quad (A3)$$

σ being the resolution power mentioned earlier [44].

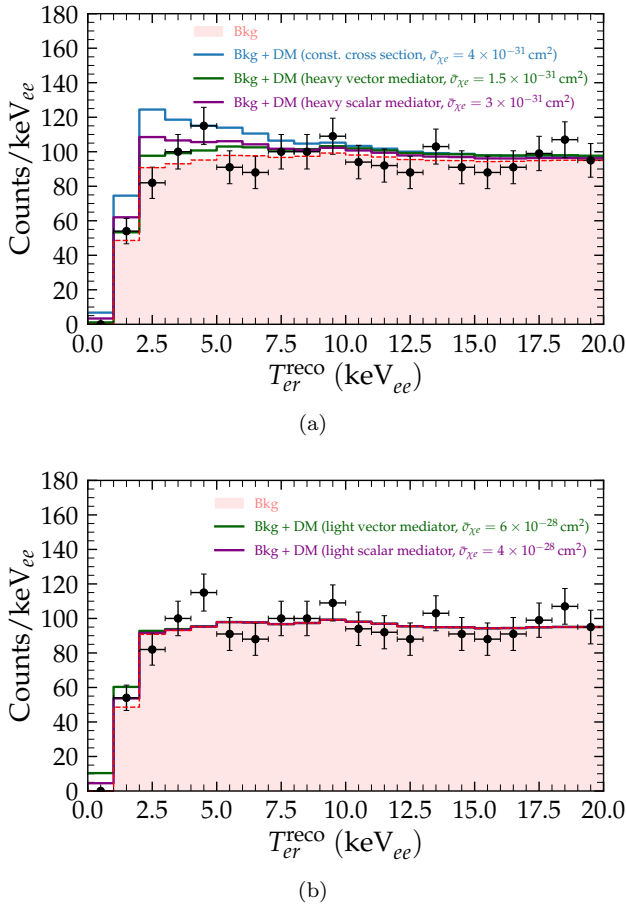


FIG. 5: Expected recoil signature of CRe boosted DM in LZ detector [13] for (a) heavy mediator with $m_\chi = 1$ MeV and (b) light mediator with $m_\chi = 0.1$ MeV.

The expected recoil signature is shown in Fig.5. The red shaded region and the black dots with error bars signify the background and observed events reported by LZ 2025 [13], respectively. In the Fig.5(a) we show the event spectra for different cross-section types with a fixed mass

$m_\chi = 1$ MeV depicted by different colored lines. The chosen cross-sections are 4×10^{-31} cm², 1.5×10^{-31} cm² and 3×10^{-31} cm² for constant (steel blue), vector (green) and scalar (magenta) mediated cross-sections, respectively. On the other hand, the recoil spectra with light mediator limit is displayed in Fig.5(b). Here we consider $m_\chi = 0.1$ MeV and $\bar{\sigma}_{\chi e} = 6 \times 10^{-28}$ cm², and 4×10^{-28} cm² for vector (green) and scalar (magenta) mediated cross-sections, respectively. It is worth noting the role of the interaction type and the mediator mass role in deciding the recoil signature in the aforementioned plots.

Appendix B: Statistical Analysis

The statistical interpretation of the LZ WS2024 data is performed using a binned spectral analysis based on a Poisson-likelihood χ^2 framework [54]. The test statistic is defined as

$$\chi^2(\vec{\mathcal{S}}; \gamma_k) = 2 \sum_i \left[R_{\text{pred}}^i(\vec{\mathcal{S}}; \gamma_k) - R_{\text{exp}}^i \right. \\ \left. + R_{\text{exp}}^i \ln\left(\frac{R_{\text{exp}}^i}{R_{\text{pred}}^i(\vec{\mathcal{S}}; \gamma_k)}\right) \right] + \sum_k \left(\frac{\gamma_k}{\sigma_{\gamma_k}} \right)^2, \quad (B1)$$

where R_{exp}^i denotes the observed number of events in the i -th recoil-energy bin, taken from Fig. 2 of Ref. [13]. The predicted event rate in each bin is obtained by combining the theoretically simulated dark matter signal ($R_{\chi e}^i(\vec{\mathcal{S}})$) with the individual background components as reported by the LZ collaboration [13], and is expressed as,

$$R_{\text{pred}}^i(\vec{\mathcal{S}}; \gamma_k) = R_{\chi e}^i(\vec{\mathcal{S}}) + (1 + \gamma_{^{214}\text{Pb}}) R_{^{214}\text{Pb} \rightarrow \beta}^i \\ + (1 + \gamma_{\text{Kr/Ar}}) R_{^{85}\text{Kr} \rightarrow ^{39}\text{Ar} + \beta + \gamma}^i \\ + (1 + \gamma_{\nu\text{ER}}) R_{\nu\odot\text{ER}}^i \\ + (1 + \gamma_{2\nu\beta\beta}) R_{^{136}\text{Xe} \rightarrow 2\nu\beta\beta}^i \\ + (1 + \gamma_{\text{Po/Pb}}) R_{^{218}\text{Po} \rightarrow ^{212}\text{Pb} \beta}^i \\ + (1 + \gamma_{\text{H/C}}) R_{^{3}\text{H} \rightarrow ^{14}\text{C}}^i \\ + (1 + \gamma_{\text{DEC}}) R_{^{124}\text{Xe} \rightarrow \text{DEC}}^i \\ + (1 + \gamma_{\text{EC}}) R_{^{127}\text{Xe} \rightarrow ^{125}\text{Xe} \beta}^i. \quad (B2)$$

The nuisance parameters γ_k encode uncertainties in the normalization of individual background components and

are constrained by Gaussian priors with widths [13]

$$\begin{aligned}\sigma_{^{214}\text{Pb}} &= \frac{130}{1099}, & \sigma_{\text{Kr/Ar}} &= \frac{33}{237}, & \sigma_{\nu\text{ER}} &= \frac{9}{151}, \\ \sigma_{2\nu\beta\beta} &= \frac{16}{107}, & \sigma_{\text{Po/Pb}} &= \frac{11.0}{92.1}, & \sigma_{\text{H/C}} &= \frac{3.4}{61.2}, \\ \sigma_{\text{DEC}} &= \frac{4.0}{20.0}, & \sigma_{\text{EC}} &= \frac{0.7}{3.2}.\end{aligned}\quad (\text{B3})$$

These nuisance parameters are marginalized over in the χ^2 minimization procedure for each choice of the new-physics parameter set $\vec{\mathcal{S}}$ i.e. each set of $\{m_\chi, \sigma_{\chi e}\}$ values.

Appendix C: DM with light scalar mediators

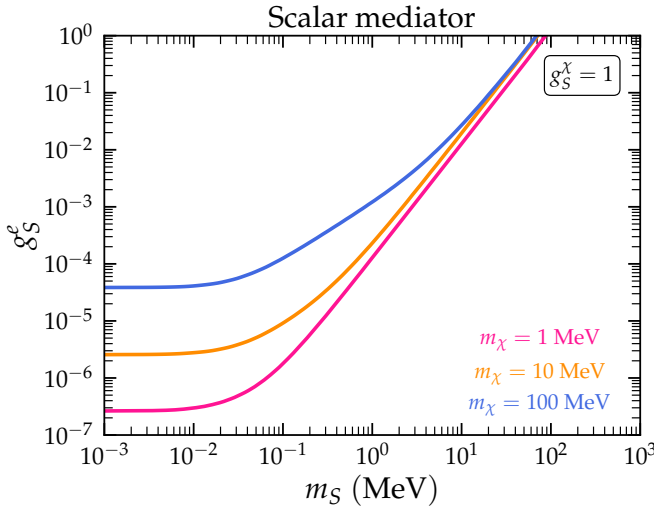


FIG. C.6: 2σ C.L. constraints in the **scalar** mediator mass vs. coupling parameter space for CRe boosted DM from LZ 2025. Limits corresponding to $m_\chi = 1$ MeV, 10 MeV and 100 MeV are represented by the region above the purple, orange and blue solid lines respectively.

Here, we choose a minimal model with fermion DM χ and a scalar mediator S with the following Yukawa like lagrangian,

$$\mathcal{L}_{\text{int}} \supset -g_S^\chi S \bar{\chi} \chi - g_S^e S \bar{e} e, \quad (\text{C1})$$

g_S^e (g_S^χ) is the respective coupling of V with electron (DM). The mediator mass is denoted as m_S . The reference NR cross-section is then given by,

$$\bar{\sigma}_{\chi e} = \frac{(g_S^e g_S^\chi)^2 \mu_{\chi e}^2}{\pi (q_{\text{ref}}^2 + m_S^2)^2} \quad (\text{C2})$$

The corresponding 2σ C.L. constraints in the scalar mediator parameter space (m_S vs. g_S^e plane) for CRe boosted DM from LZ 2025 is presented in Fig.C.6. Here, we also fix the DM coupling g_S^χ to be 1 and showcase our exclusion limits for $m_\chi = 1$ MeV, 10 MeV and 100 MeV depicted by the regions above the purple, orange and blue solid lines respectively.

[1] G. Jungman, M. Kamionkowski and K. Griest, *Supersymmetric dark matter*, *Phys. Rept.* **267** (1996) 195–373, [[hep-ph/9506380](#)].

[2] M. Cirelli, A. Strumia and J. Zupan, *Dark Matter*, [2406.01705](#).

[3] F. Zwicky, *Die Rotverschiebung von extragalaktischen Nebeln*, *Helv. Phys. Acta* **6** (1933) 110–127.

[4] V. C. Rubin and W. K. Ford, Jr., *Rotation of the Andromeda Nebula from a Spectroscopic Survey of Emission Regions*, *Astrophys. J.* **159** (1970) 379–403.

[5] PAMELA collaboration, O. Adriani et al., *The cosmic-ray electron flux measured by the PAMELA experiment between 1 and 625 GeV*, *Phys. Rev. Lett.* **106** (2011) 201101, [[1103.2880](#)].

[6] PLANCK collaboration, N. Aghanim et al., *Planck 2018 results. VI. Cosmological parameters*, *Astron. Astrophys.* **641** (2020) A6, [[1807.06209](#)].

[7] T. Lin, *Dark matter models and direct detection*, *PoS* **333** (2019) 009, [[1904.07915](#)].

[8] J. L. Feng, *Dark Matter Candidates from Particle Physics and Methods of Detection*, *Ann. Rev. Astron. Astrophys.* **48** (2010) 495–545, [[1003.0904](#)].

[9] D. Aristizabal Sierra, V. De Romeri, L. J. Flores and D. K. Papoulias, *Impact of COHERENT measurements, cross section uncertainties and new interactions on the neutrino floor*, *JCAP* **01** (2022) 055, [[2109.03247](#)].

[10] V. De Romeri, A. Majumdar, D. K. Papoulias and R. Srivastava, *New light mediators and the neutrino fog: Implications from XENONnT nuclear recoil data*, [2512.08853](#).

[11] XENON collaboration, E. Aprile et al., *Energy resolution and linearity of XENON1T in the MeV*

energy range, *Eur. Phys. J. C* **80** (2020) 785, [2003.03825].

[12] LZ collaboration, J. Aalbers et al., *First Dark Matter Search Results from the LUX-ZEPLIN (LZ) Experiment*, *Phys. Rev. Lett.* **131** (2023) 041002, [2207.03764].

[13] LZ collaboration, D. S. Akerib et al., *Search for New Physics via Low-Energy Electron Recoils with a 4.2 Tonne \times Year Exposure from the LZ Experiment*, 2511.17350.

[14] PANDAX collaboration, M. Zhang et al., *Search for Light Dark Matter with 259 Days of Data in PandaX-4T*, *Phys. Rev. Lett.* **135** (2025) 211001, [2507.11930].

[15] DARKSIDE collaboration, P. Agnes et al., *Constraints on Sub-GeV Dark-Matter-Electron Scattering from the DarkSide-50 Experiment*, *Phys. Rev. Lett.* **121** (2018) 111303, [1802.06998].

[16] T. Bringmann and M. Pospelov, *Novel direct detection constraints on light dark matter*, *Phys. Rev. Lett.* **122** (2019) 171801, [1810.10543].

[17] Y. Ema, F. Sala and R. Sato, *Light Dark Matter at Neutrino Experiments*, *Phys. Rev. Lett.* **122** (2019) 181802, [1811.00520].

[18] J. B. Dent, B. Dutta, J. L. Newstead and I. M. Shoemaker, *Bounds on Cosmic Ray-Boosted Dark Matter in Simplified Models and its Corresponding Neutrino-Floor*, *Phys. Rev. D* **101** (2020) 116007, [1907.03782].

[19] J. B. Dent, B. Dutta, J. L. Newstead, I. M. Shoemaker and N. T. Arellano, *Present and future status of light dark matter models from cosmic-ray electron upscattering*, *Phys. Rev. D* **103** (2021) 095015, [2010.09749].

[20] D. Bardhan, S. Bhowmick, D. Ghosh, A. Guha and D. Sachdeva, *Bounds on boosted dark matter from direct detection: The role of energy-dependent cross sections*, *Phys. Rev. D* **107** (2023) 015010, [2208.09405].

[21] N. F. Bell, M. J. Dolan and S. Robles, *Searching for Sub-GeV Dark Matter in the Galactic Centre using Hyper-Kamiokande*, *JCAP* **09** (2020) 019, [2005.01950].

[22] D. K. Ghosh, T. Gupta, M. Heikinheimo, K. Huitu and S. Jeesun, *Boosted dark matter driven by cosmic rays and diffuse supernova neutrinos*, *Phys. Rev. D* **111** (2025) 063019, [2411.11973].

[23] J.-W. Wang, A. Granelli and P. Ullio, *Direct Detection Constraints on Blazar-Boosted Dark Matter*, *Phys. Rev. Lett.* **128** (2022) 221104, [2111.13644].

[24] S. Jeesun, *Blazar boosted ALP and vector portal dark matter confronting light mediator searches*, *Phys. Rev. D* **111** (2025) 103022, [2501.11569].

[25] A. G. De Marchi, A. Granelli, J. Nava and F. Sala, *Boosted dark matter versus dark matter-induced neutrinos from single and stacked blazars*, *JHEP* **12** (2025) 136, [2507.12278].

[26] A. Das and M. Sen, *Boosted dark matter from diffuse supernova neutrinos*, *Phys. Rev. D* **104** (2021) 075029, [2104.00027].

[27] V. De Romeri, A. Majumdar, D. K. Papoulias and R. Srivastava, *XENONnT and LUX-ZEPLIN constraints on DSNB-boosted dark matter*, *JCAP* **03** (2024) 028, [2309.04117].

[28] B. Bhalla, F. Hajkarim, D. Kim and K. Sinha, *Supernova-Boosted Dark Matter at Large-Volume Neutrino Detectors*, 2506.15765.

[29] H. An, M. Pospelov, J. Pradler and A. Ritz, *Directly Detecting MeV-scale Dark Matter via Solar Reflection*, *Phys. Rev. Lett.* **120** (2018) 141801, [1708.03642].

[30] T. Emken, R. Essig and H. Xu, *Solar reflection of dark matter with dark-photon mediators*, *JCAP* **07** (2024) 023, [2404.10066].

[31] D. Ghosh, A. Guha and D. Sachdeva, *Exclusion limits on dark matter-neutrino scattering cross section*, *Phys. Rev. D* **105** (2022) 103029, [2110.00025].

[32] A. Das, T. Herbermann, M. Sen and V. Takhistov, *Energy-dependent boosted dark matter from diffuse supernova neutrino background*, *JCAP* **07** (2024) 045, [2403.15367].

[33] M. J. Boschini et al., *Solution of heliospheric propagation: unveiling the local interstellar spectra of cosmic ray species*, *Astrophys. J.* **840** (2017) 115, [1704.06337].

[34] J. F. Navarro, C. S. Frenk and S. D. M. White, *A Universal density profile from hierarchical clustering*, *Astrophys. J.* **490** (1997) 493–508, [astro-ph/9611107].

[35] A. Guha and J.-C. Park, *Constraints on cosmic-ray boosted dark matter with realistic cross section*, *JCAP* **07** (2024) 074, [2401.07750].

[36] SUPERCDMS collaboration, R. Agnese et al., *First Dark Matter Constraints from a SuperCDMS Single-Charge Sensitive Detector*, *Phys. Rev. Lett.* **121** (2018) 051301, [1804.10697].

[37] SENSEI collaboration, M. Crisler, R. Essig, J. Estrada, G. Fernandez, J. Tiffenberg, M. Sofo haro et al., *SENSEI: First Direct-Detection Constraints on sub-GeV Dark Matter from a Surface Run*, *Phys. Rev. Lett.* **121** (2018) 061803, [1804.00088].

[38] R. Essig, A. Manalaysay, J. Mardon, P. Sorensen and T. Volansky, *First Direct Detection Limits on sub-GeV Dark Matter from XENON10*, *Phys. Rev. Lett.* **109** (2012) 021301, [1206.2644].

[39] A. C. Cummings, E. C. Stone, B. C. Heikkila, N. Lal, W. R. Webber, G. Jóhannesson et al., *Galactic Cosmic Rays in the Local Interstellar Medium: Voyager 1 Observations and Model Results*, *Astrophys. J.* **831** (2016) 18.

[40] FERMI-LAT collaboration, M. Ackermann et al., *Measurement of separate cosmic-ray electron and positron spectra with the Fermi Large Area Telescope*, *Phys. Rev. Lett.* **108** (2012) 011103, [1109.0521].

[41] AMS collaboration, M. Aguilar et al., *Precision Measurement of the $(e^+ + e^-)$ Flux in Primary Cosmic Rays from 0.5 GeV to 1 TeV with the Alpha Magnetic Spectrometer on the International Space Station*, *Phys. Rev. Lett.* **113** (2014) 221102.

[42] M. J. Boschini et al., *HelMod in the works: from direct observations to the local interstellar spectrum of cosmic-ray electrons*, *Astrophys. J.* **854** (2018) 94, [1801.04059].

[43] J.-W. Chen, H.-C. Chi, C. P. Liu and C.-P. Wu, *Low-energy electronic recoil in xenon detectors by solar neutrinos*, *Phys. Lett. B* **774** (2017) 656–661, [1610.04177].

[44] LZ collaboration, G. Pereira, C. Silva and V. N. Solovov, *Energy resolution of the LZ detector for high-energy electronic recoils*, *JINST* **18** (2023) C04007.

[45] DAMIC-M collaboration, K. Aggarwal et al., *Probing Benchmark Models of Hidden-Sector Dark Matter with DAMIC-M*, *Phys. Rev. Lett.* **135** (2025) 071002,

[2503.14617].

- [46] C. V. Cappiello, Q. Liu, G. Mohlabeng and A. C. Vincent, *Cosmic ray-boosted dark matter at IceCube*, *Phys. Rev. D* **110** (2024) 095031, [[2405.00086](#)].
- [47] E. Hardy and R. Lasenby, *Stellar cooling bounds on new light particles: plasma mixing effects*, *JHEP* **02** (2017) 033, [[1611.05852](#)].
- [48] Y.-D. Tsai, J. Eby, J. Arakawa, D. Farnocchia and M. S. Safronova, *OSIRIS-REx constraints on local dark matter and cosmic neutrino profiles*, *JCAP* **02** (2024) 029, [[2210.03749](#)].
- [49] S. Knapen, T. Lin and K. M. Zurek, *Light Dark Matter: Models and Constraints*, *Phys. Rev. D* **96** (2017) 115021, [[1709.07882](#)].
- [50] G. Krnjaic and S. D. McDermott, *Implications of BBN Bounds for Cosmic Ray Upscattered Dark Matter*, *Phys. Rev. D* **101** (2020) 123022, [[1908.00007](#)].
- [51] BABAR collaboration, J. P. Lees et al., *Search for a Dark Photon in e^+e^- Collisions at BaBar*, *Phys. Rev. Lett.* **113** (2014) 201801, [[1406.2980](#)].
- [52] M. Bauer, P. Foldenauer and J. Jaeckel, *Hunting All the Hidden Photons*, *JHEP* **07** (2018) 094, [[1803.05466](#)].
- [53] D. Banerjee et al., *Dark matter search in missing energy events with NA64*, *Phys. Rev. Lett.* **123** (2019) 121801, [[1906.00176](#)].
- [54] F. M. L. Almeida, Jr., M. Barbi and M. A. B. do Vale, *A Proposal for a different chi square function for Poisson distributions*, *Nucl. Instrum. Meth. A* **449** (2000) 383–395, [[hep-ex/9911042](#)].